Static and dynamic profiles of tethered polymer layers probed by analyzing the noise of an atomic force microscope

Andreas Roters, Martin Gelbert, Martin Schimmel, Jürgen Rühe, and Diethelm Johannsmann*
Max-Planck-Institute of Polymer Research, Ackermannweg 10, 55128 Mainz, Germany
(Received 19 March 1997)

We have analyzed the thermal noise of the cantilever of an atomic force microscope, which is dominated by Brownian motion. The noise power spectra display the resonance properties of the cantilever, and are influenced by the cantilevers immediate environment. Fitting Lorentzians to the noise power spectra, we can derive a friction coefficient, an effective spring constant, and an effective mass. The dc force onto the cantilever is obtained from the static offset. When approaching the cantilever to surfaces covered with tethered polymer layers, we find a strong increase in the friction coefficient. We ascribe this to the breathing mode. At shorter distances there is an increase in spring constant indicative of an elastic interaction. The dc force and the effective spring constant show markedly different behavior. [S1063-651X(97)06209-0]

PACS number(s): 61.16.Ch, 61.25.Hq, 68.45.Nj, 81.40.Pq

INTRODUCTION

Polymeric adsorbates at surfaces play an important role in many areas of technology such as colloid stabilization [1], adhesion [2], lubrication [3], tribology [4], chromatography [5], and rheology [6]. The physical properties of biopolymers attached to the cell surface are crucial for the structure, the stability, and most notably the interaction of the cell with its environment [7]. The structure and dynamics of such polymeric adsorbates as well as their response to perturbations has therefore attracted a great deal of scientific interest [8]. ''Tethered layers,'' which are systems of terminally grafted linear polymer chains, have been intensely investigated [9–12]. For a sufficiently high grafting density there is strong lateral chain overlap and the increase in osmotic pressure leads to chain stretching [13,14]. These systems are called polymer brushes. The covalent attachment at one end makes brushes a clean model system. On the other hand, the peculiar boundary conditions of terminal attachment lead to a polymer conformation and dynamics different from polymers in the bulk.

Considerable understanding has been gained in the past about the structure of neutral polymer brushes. Data obtained with neutron scattering [15,16] and reflection [17,18], mean-field calculations [19–21], and numerical simulations [22–25] have resulted in a fairly consistent picture of polymer brushes immersed in solvents of varying quality. Less is known about the dynamics and the interaction of brushes with—for instance—an immersed hard sphere, an opposing wall [26–28], shear flow [4,29–31], or another brush [26,27]. The surface forces apparatus (SFA) has been used to probe some of these interactions [26–28]. For example, Taunton *et al.* [26] found a monotonous repulsion between two brushes extending to a range roughly corresponding to the length of the adsorbed chains.

It has been realized for a while that the atomic force microscope (AFM) [32] has a great deal of conceptual similarity to the surface forces apparatus. The advantages lie in the lateral resolution and speed. In this work we build on the speed advantage to obtain dynamic information. On the other hand, forces and the distances are harder to quantify in the AFM than in the SFA. Difficulties in accounting for the tip geometry are another source of complication. Soft surfaces exerting only weak forces onto the tip such as polymer brushes or living cells are difficult to image [4]. The tip easily penetrates into the sample. Force modulation [33,34], the ''noncontact mode'' [35], and the ''tapping mode'' [36,37] have been shown to circumvent these problems to some extent, either by relying on dynamic interactions or by reducing the time of contact.

Noise analysis can be used in a variety of ways to obtain information on either the AFM cantilever [38–42] or the tip-sample interaction [43]. In a recent publication [44] we showed that measuring the thermal noise spectrum of the cantilever is another way to obtain both dynamic and static information on soft samples. Figure 1 illustrates the principle. Instead of actively modulating the cantilever, we rely on its Brownian motion. Noise measurements have a number of advantages. They can be done with any AFM instrument without additional equipment. They minimize the disturbance to the sample. Most prominently, the multiplex advantage is gained because information is extracted simulta-

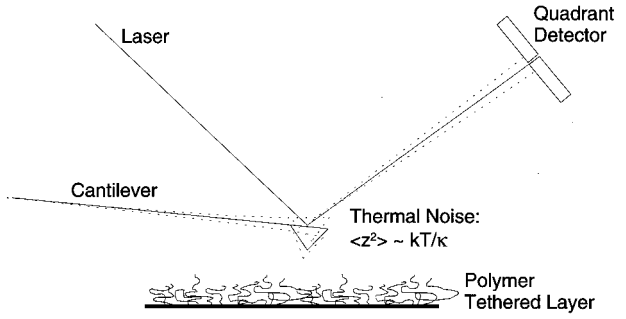

FIG. 1. Schematic description of the experimental setup.

*Author to whom correspondence should be addressed.
Fax: 49-6131-379 360.
Electronic address: johannsmann@mpip-mainz.mpg.de

neously from a bandwidth of about 25 kHz. We make use of this ''multiplex advantage'' in two ways. First, we can easily recognize and discard experimentally anomalous situations because they result in an irregular noise spectrum. The Lorentzians contain the effective mass as a fit parameter, which is not obtainable with active modulation techniques. The low amplitude ensures that we are in the regime of linear response, which is not necessarily true for the tapping mode. Finally, we can directly obtain the spectrum of frequency-dependent friction, which opens the way to local dynamic spectroscopy. We will treat this aspect in a separate publication [45].

The most severe disadvantage of the technique is the possibility of nonthermal noise sources. Electronic noise at discrete frequencies, however, is easily noticed and can be either subtracted or eliminated. We checked for nonthermal acoustic noise by deliberately introducing it, and found that it is much smaller than thermal noise under standard conditions. Some $1/f$ noise at low frequencies, on the other hand, can usually not be eliminated. Frequencies less than about 200 Hz therefore have to be analyzed with caution. Another limitation for noise measurements is that they can only be done with soft cantilevers. Because the thermal rms displacement $\langle z^2\rangle^{1/2}$ depends on the inverse of the spring constant κ through $\langle z^2\rangle \propto kT/\kappa$ [40], the Brownian noise is covered by nonthermal noise, if the spring constant is too high.

Interestingly, elastically suspended mirrors in a gaseous environment were used in the 1920s to study Brownian motion. Experiments in liquids are more complicated because of the hydrodynamic aspect. Fluid backflow introduces a long-time tail in the autocorrelation function [46]. The effective mass is not the mass of the mirror alone. For complicated geometries such as a cantilever immersed into a polymer brush, a rigorous treatment is impossible, and hydrodynamic effects are a major problem in the analysis. Note, however, that all other dynamic modes of the atomic force microscope have to deal with hydrodynamics in the same way. The small amplitudes of motion encountered in noise measurements are even advantageous because they ensure low Reynolds numbers [44].

We reported on the noise spectrum in liquids and gases of different densities and viscosities as well as the on the behavior when approaching the cantilever to a solid surface [44]. A hydrodynamic coupling of the cantilever to the surface was observed at tip-sample distances which roughly correspond to the dimension of the cantilever. This coupling only affects the friction coefficient. In the present publication we show that surfaces covered by thick polymer brushes affect the noise spectra of AFM cantilevers much differently than a hard glass surface. Thick polymer brushes display an extended transition region where the dynamic properties continuously vary from rubbery to liquid. We believe that many other soft surfaces display a similar transition region.

The tethered layers studied here were prepared by the ''grafting-from'' approach [47–50], in which the polymer is formed *in situ* at the surface of the substrate by radical chain polymerization from a self-assembled monolayer of an initiator. The grafting-from procedure is particularly successful with respect to the achievable grafting densities and layer thicknesses. It by far exceeds those obtained with ''grafting-to'' procedures, where preformed polymers are reacted with appropriate surface sites. The reason is that for grafting from the limiting factor is the diffusion of monomers towards a growing chain rather than diffusion of polymers to the surface. Following the grafting from approach, polymer molecules with molecular weights up to $M_w = 5\times 10^6$ g/mol have been attached to the surfaces with high graft densities. Films with thicknesses of more than one μm in the dry state have been obtained. The molecular weights of the polymers can be measured after cleaving an ester bond, which is part of the anchor group.

We show viscoelastic profiles on three poly-(methylmethacrylate) (PMMA) tethered layers with dry thicknesses of 5, 28, and 190 nm as well as an empty sample for reference. The ambient medium was toluene. When tethered layers are immersed into a solvent, the osmotic pressure induces swelling. In equilibrium the osmotic pressure is balanced by the tensile force of the stretched chains [13,14]. There are numerous theoretical and experimental studies on the response of a swollen brush to vertical compression by either a flat surface or another brush [26–28,51,52]. The response to an approaching AFM tip was recently investigated by Overney *et al.* [53]. Murat and Grest [54] performed a molecular-dynamics simulation modeling this experiment. Overney *et al.* [53] presented data on the static forces and on the response to a 3-kHz modulation of the tip height. The response to the ac modulation was quite irregular. Apparently, the ac modulation constitutes a severe disturbance of the brush leading to fluctuating structural rearrangements. As we show below, noise measurements are more suitable for dynamic investigations on polymer brushes because the dynamic disturbance is minimized. We obtained smooth profiles of the viscous and the elastic modulus of compression.

THEORY

We model the cantilever as an elastically suspended sphere which experiences random forces from its environment [55]. The statistical motion of such a particle is described by the Langevin equation

$$\frac{d^2z(t)}{dt^2}+\gamma\frac{dz(t)}{dt}+\omega_0^2 z(t)=\frac{1}{m}R(t), \tag{1}$$

where z is the displacement, $\omega_0=(\kappa/m)^{1/2}$ the eigenfrequency, $\gamma=\xi/m$ the damping constant, ξ the friction coefficient, κ the spring constant, m the mass, and $R(t)$ the random force. In Newtonian liquids the power spectrum of the random force does not depend on frequency. The parameters γ, ω_0, and m are effective parameters which depend on the cantilever's environment. By virtue of the fluctuation-dissipation theorem the noise power spectrum $d|z^2|/d\omega$ corresponds to the imaginary part of the cantilever's mechanical susceptibility and is

$$\frac{d|z^2|}{d\omega}=\frac{A\gamma}{(\omega_0^2-\omega^2)^2+\gamma^2\omega^2}=\frac{kT}{\pi m}\frac{\gamma}{(\omega_0^2-\omega^2)^2+\gamma^2\omega^2}, \tag{2}$$

with $A=kT/\pi m$ the oscillator strength and kT the thermal energy. From the quantities A, ω_0, and γ we can derive the effective mass m, the effective spring constant κ, and the friction coefficient ξ as

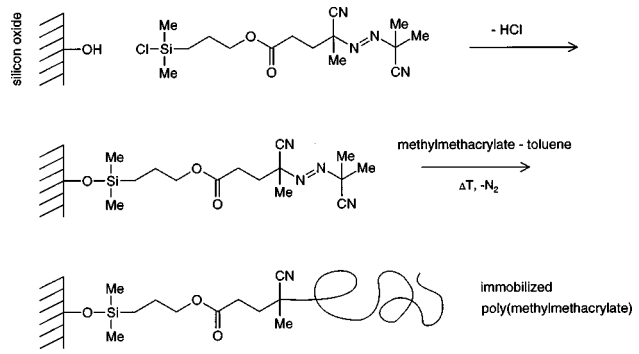

FIG. 2. Synthesis of tethered polymer layers by the ''grafting from'' approach. The initiator is self-assembled on a silicon oxide surface. The polymer grows *in situ* by free radical polymerization from that surface-bound initiator.

$$m = \frac{kT}{\pi A}, \tag{3a}$$

$$\kappa = \omega_0^2 \frac{kT}{\pi A}, \tag{3b}$$

$$\xi = \gamma \frac{kT}{\pi A}. \tag{3c}$$

A fourth parameter automatically obtained is the dc force F_{dc}, which is proportional to the time-averaged displacement of the cantilever. Here we focus on the fact that the effective parameters depend on the cantilever's environment. The friction coefficient ξ is often expressed as $\xi = 6\pi\eta R$ with R the hydrodynamic radius of a hypothetical equivalent sphere and η the viscosity. For a cantilever the hydrodynamic situation is more complicated. However, the friction coefficient still is a measure of the local viscosity.

MATERIALS

The synthesis of the polymer tethered layers followed the ''grafting from'' approach as depicted in Fig. 2. Details are described in Refs. [47–50]. Table I summarizes the conditions of polymerization and the properties of the different samples. Briefly, the first step is the immobilization of an initiator for free radical polymerization at the surface of a silicon wafer. Other oxidic substrates can be used as well. The initiator used is a derivative of azo-bisisobutylnitrile (AIBN), which is attached to the wafer via a monochlorsilyl moiety. Subsequently, the polymerization is thermally initiated in a solution of monomer. We report on PMMA tethered layers. After polymerizing for some hours at 60 °C, the samples are rinsed with solvent and undergo Soxhlet extraction for 15 h to remove physisorbed polymer. The dry thicknesses are determined by surface plasmon spectroscopy [56] and waveguide spectroscopy [57]. The molecular weight of a given sample is *a priori* unknown. However, we can infer the molecular weight from other experiments using large substrates as well as high surface area silica gels. The grafted polymer was cleaved off the surface after polymerization and investigated with size exclusion chromatography and static light scattering. For sample PMMA190, these measurements yield $M_w = 800\,000$ g/mol. For thinner layers, the molecular weights given in Table I have been inferred from other experiments with analogous conditions but larger surfaces to obtain more amount for analysis. The polydispersity typically is in the range of $M_w/M_n = 2-3$. From the total mass and the molecular weight the number of chains per unit surface and the distance between two grafting sites can be estimated. The dimensionless grafting density $\sigma < 1$, which is the ratio of the minimum area per segment divided by the area per chain is another useful number. While samples PMMA28 and PMMA190 clearly are well in the brush regime, sample PMMA5 is closer to what should be called a ''mushroom'' because the overlap between adjacent chains is quite small.

EXPERIMENTAL PROCEDURE AND DATA ANALYSIS

Details of the experimental procedure were published in Ref. [44]. Figure 1 schematically depicts the principle. The instrument was a TMX 2010 from TopoMetrix. We used *V*-shaped silicon nitride cantilevers. The tip has the shape of a pyramid with an opening angle of about 70°. The height of the pyramid is about 2.9 μm. It should be kept in mind that a large part of the tip interacts with the polymer layers. Therefore the tip radius at the end is of minor importance.

The rms noise $\langle z^2 \rangle^{1/2}$ is about 3 Å. It is easily detected. Only the fundamental resonance was in the accessible range of frequencies. In air the resonance frequencies typically are about 40 kHz with a Q factor of about 20. In liquids the resonance frequencies decrease to about 10 kHz and the Q factors are about 2.

For determining the viscoelastic profile we worked in a liquid cell. The vertical tip-sample distance is adjusted by the z piezo of the scanner, while the x and y piezos are discon-

TABLE I. Material parameters for the tethered layers.

Sample	PMMA5	PMMA28	PMMA190
polymerization temperature	60 °C	60 °C	60 °C
monomer concentration	4.96 M	4.96 M	4.96 M
polymerization time	0.42 h	1.5 h	8 h
molecular weight M_w	20 000 g/mol	120 000 g/mol	800 000 g/mol
grafting distance	14 nm	7 nm	3 nm
dimensionless grafting density	0.003	0.01	0.06
dry layer thickness	5 nm	28 nm	190 nm

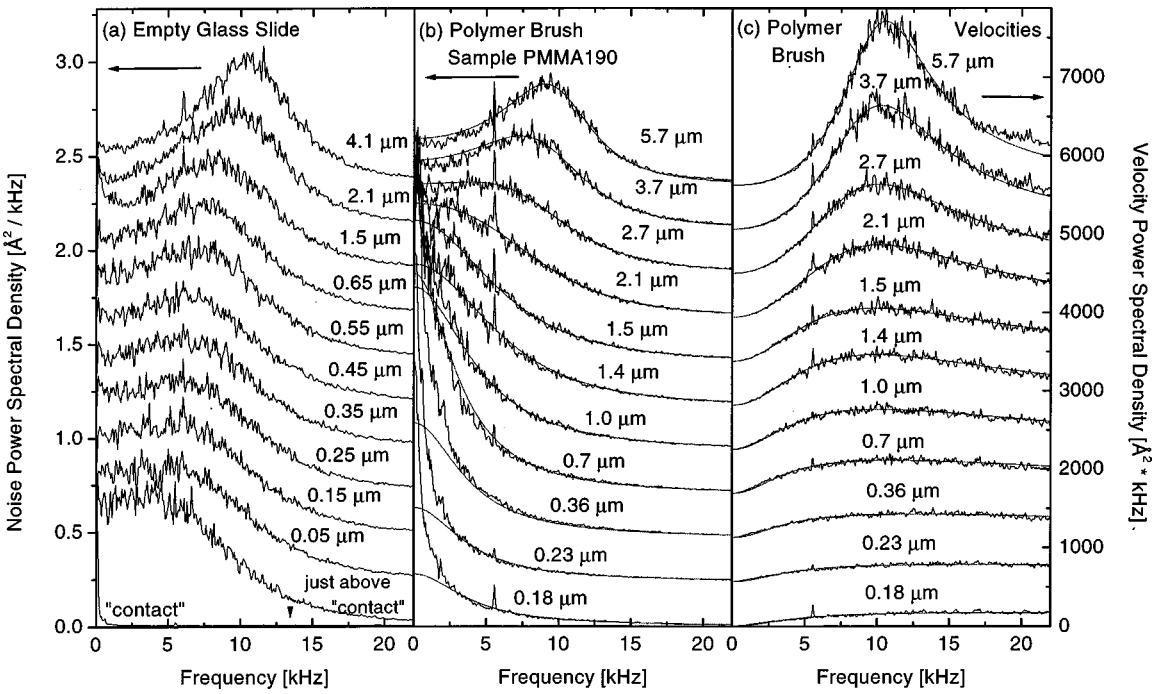

FIG. 3. Noise spectra obtained during the approach to sample PMMA190 (b) and an empty glass slide (a). The numbers in the figure give the tip-sample distance. The noise spectra are influenced by the presence of a surface in both cases. However, the effects are much stronger for a cantilever touching a brush. (c) displays the same data as (b) as velocity spectra. Velocity spectra are more easily visually analyzed than the displacement spectra. The low frequency excess noise in part (b) is attributed to viscoelastic relaxation [45].

nected. We had to include a low pass filter with a cutoff around 150 Hz into the driving electronics of the z piezo to get rid of the noise from the piezo driver. The ''pictures'' taken in that configuration contain only noise. The sampling rate was 32 kHz (limited by the instrument). At frequencies higher than about 25 kHz the fits show that the data are affected by aliasing [58]. We therefore do not show data from frequencies above 25 kHz. We took one ''picture'' containing 131 072 pixels (corresponding to a data acquisition time of 4 s) for each height. All pictures were taken in approach, i.e., the profiles were measured with the height decreasing between successive data points.

Before doing the Fourier transformation, we subtracted a straight line from each data string in the time domain. In that way both the static offset and a linear instrumental drift are eliminated from the analysis. The drift mainly originates from a relaxation of the z piezo after changing its driving voltage. The static offset can be converted to a dc force and is one of the parameters of interest in the profile determination.

The spectral noise power density is obtained by Fourier transformation of data strings of 1024 pixels each. We used an algorithm from ''numerical recipes'' [58] with suitable apodization. In general, apodization is uncritical because the data do not contain narrow lines. Parallel to data taking we monitored the noise with a Fourier analyzer (HP 35670A) connected to the analog output of the quadrant detector. After moving the sample stage we observed some irregular excess noise, which usually disappeared within a few seconds. Therefore we waited 4 s after each movement of the sample stage to allow for equilibration.

The statistical error on the noise spectra is in the range of 10%. Although the statistical error can certainly be reduced by longer integration, slow measurements suffer from instrumental drifts. Altogether, data acquisition for one distance profile such as the ones displayed in Fig. 4 takes about 4 min.

Height calibration is not trivial. For sufficiently thin layers, there is a well-defined kink in the force-distance curve which is a good choice for zero distance $D=0$. At that same height, the thermal noise discontinuously disappears leaving only nonthermal noise at discrete frequencies. The interpretation is that for sufficiently thin layers, the tip can dive into the layer until it touches the substrate at some discrete height $D=0$. Although the ''dynamic'' procedure is independent from the procedure using the force-distance curve, the values coincide for sufficiently thin layers. For thick and dense brushes like sample PMMA190, neither method works well. Both the slope of the force distance curve and the noise amplitude continuously approach their final values. No clear point of ''contact'' can be identified. Apparently, the tip cannot touch the bottom of thick brushes in the same way as for thin layers. There is a genuine uncertainty in the origin of the D scale for these thick brushes. For sample PMMA190 we estimate this uncertainty to less then 50 nm, which is quarter of the dry thickness.

The analysis critically requires that the origin of noise is indeed the thermal Langevin force [59]. Any electronic noise is much lower than the mechanical noise as evidenced when looking at cantilevers sitting on a solid surface. Sometimes there are electronic peaks in the spectrum [cf. the small peak around 5 kHz in Fig. 3(b)] which can be recognized and subtracted.

We can infer that the nonthermal noise is not dominant from the fact that the spring constants calculated from ther-

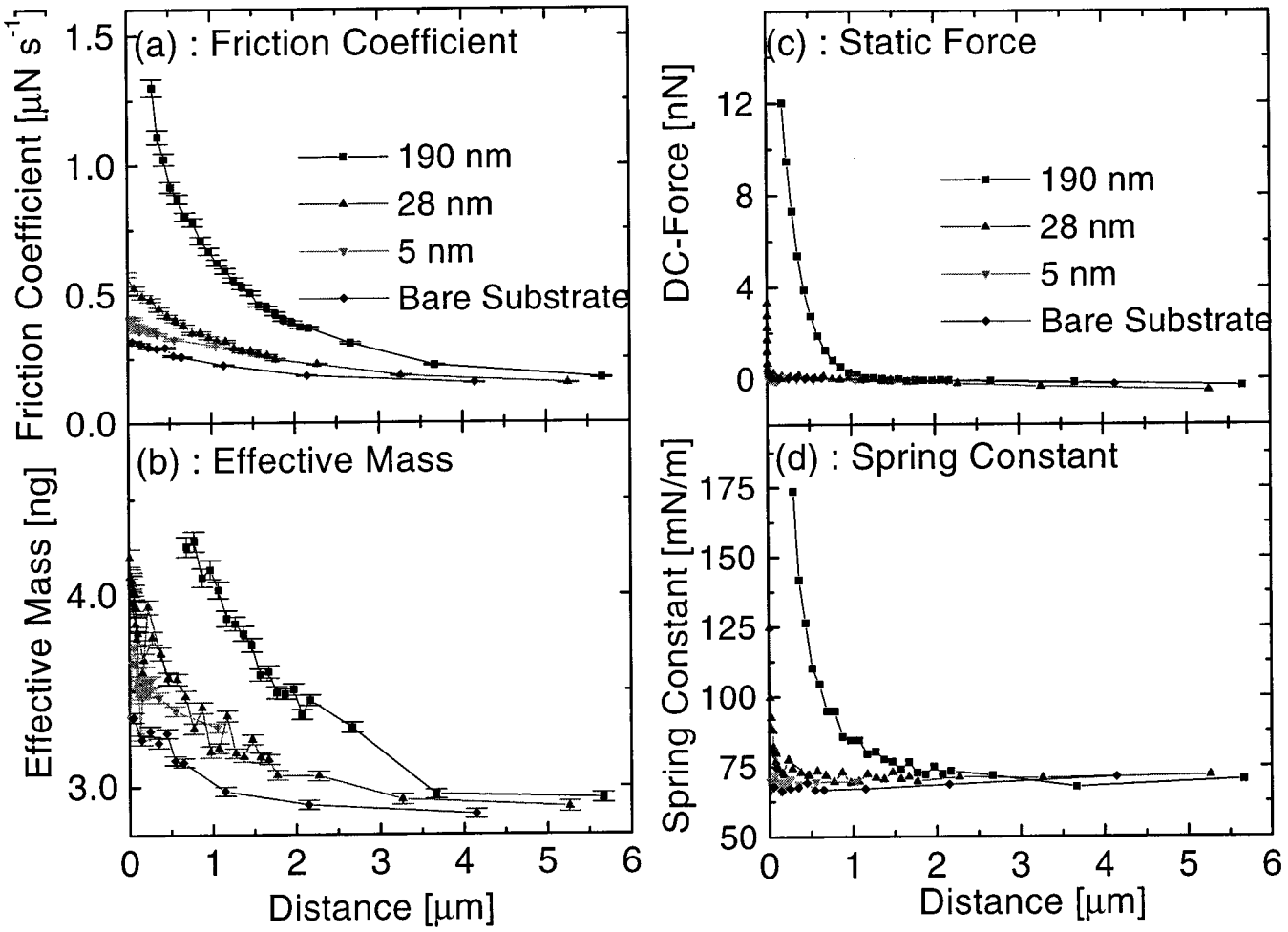

FIG. 4. Profiles of friction coefficient ξ (a), effective mass m (b), dc force (c), and effective spring constant κ (d).

mal noise roughly match the values calculated according to Ref. [60]. We focus our investigations on changes of the noise spectrum, when the cantilever approaches the sample, rather than on absolute numbers. Nonthermal noise does not critically affect our conclusions.

RESULTS AND DISCUSSION

Figure 3(b) shows a typical set of noise spectra taken on sample PMMA 190 for various tip-sample distances. For comparison the noise spectra for an empty sample are given in Fig. 3(a). While the resonance is clearly visible at large tip-sample distances, the cantilever is highly overdamped when the tip is immersed into the brush. Evidently, the damping is much stronger for brushes than for the empty glass slide.

The features of overdamped Lorentzians are more easily recognized, when the noise spectrum of velocities is displayed instead of the displacement noise. In the frequency domain this simply amounts to a multiplication with ω^2. Figure 3(c) shows the same data as Fig. 3(b) displayed as noise of velocities. Discussing velocity spectra rather than displacement spectra has the following advantages.

(i) The maximum occurs at exactly $\omega_{\max}=\omega_0$, as opposed to $\omega_{\max}=(\omega_0^2-\gamma^2/2)^{1/2}$ for the displacement spectra.

(ii) The half-band-width is equal to γ.

(iii) The noise power at maximum is $(d|v|^2/d\omega)_{\max}=A/\gamma=kT/\pi\xi$.

(iv) In the limit of $\gamma \gg \omega_0$ (highly overdamped oscillation) the fit does no longer sensitively depend on ω_0 because the velocity spectrum is very flat at the maximum. The half-band-width cannot be read either, because the high-frequency wing of the maximum extends beyond the sampling rate. However, the noise amplitude at maximum, which is $A/\gamma=kT/\pi\xi$, is well measured. Also, the curvature at low frequencies, which is ξ/κ^2, still is precisely determined. Therefore both ξ and κ are determined with small error bars even in the overdamped case. The sensitivity to the effective mass, however, is lost in the overdamped case. The inertial term in the Langevin equation becomes negligible in very viscous environments.

Because the features of the velocity spectra like peak position, peak maximum, and bandwidth are in a simple way connected to the fit parameters, the velocity spectra can be visually inspected. For example, one can directly read from Fig. 3(c) that $\omega_0=(\kappa/m)^{1/2}$ increases below $D=0.5\ \mu$m. These conveniences go back to the fact that in the overdamped case the motion of the cantilever approaches the Brownian motion of a quasifree test particle. For Brownian

motion, particle velocity is the quantity of interest rather than particle position.

The fits in Fig. 3(b) are Lorentzians. In the low-frequency range the data points lie above the fits. In a forthcoming publication [45] we argue that this is indicative of viscoelastic dispersion. Here we neglect viscoelasticity and use simple Lorentzians [Eqs. (2) and (3)]. During the minimization of χ^2 we assumed that the cantilever noise is Gaussian, which implies an error bar of 9% on each data point. An error of 9% corresponds to $(128)^{-1/2}$, 128 being the number of averaged data strings. In order to obtain small error bars on the fit parameters of the Lorentzians, we had to apply an additional statistical weight which reduces the influence of the low-frequency anomalies. We chose that statistical weight to be proportional to ω^2. This is equivalent to fitting the velocity spectra with no weight at all. These fits are displayed in Fig. 3(c).

From fits like the ones shown in Fig. 3, we obtain distance profiles of the friction coefficient ξ, the effective mass m, and the spring constant κ. The DC force F_{dc} is obtained from the static offset. Figure 4 shows the derived parameters for three PMMA tethered layers with dry thicknesses of 5, 28, and 190 nm as well as data taken on an empty glass slide. The distance D was taken from the driving voltage of the z piezo, where a correction for the cantilever displacement was applied.

One could formally convert the friction coefficient to a local viscosity using the equation $\xi = 6\pi\eta R$, which holds for sphere in stationary flow of homogeneous solvent. However, because the geometry is so complicated we do not think that this conversion of data gives any new insight. Generally speaking, the cantilever's hydrodynamic radius derived from the friction coefficient at infinite distance and the viscosity of toluene ($\eta_{\mathrm{Tol}} \sim 0.6$ cP) [61] is 30 μm, which matches the dimension of the cantilever.

The profiles given in Fig. 4 quantify various interactions between the tethered layers and the tip. We find strong effects for sample PMMA190, and weaker (but significant) effects for sample PMMA28. For sample PMMA5 the differences from an empty glass slide are quite marginal. No elastic interaction is observed at all. Since sample PMMA5 is dilute (grafting distance 140 Å), such a weak interaction is reasonable. We searched for a time evolution of the fit parameters by doing fits on subsequent subsets of the data. We did not find any systematic drift during the 4 s of data acquisition. We always took data at different spots of the sample and found only slight variations, which we do not discuss in the following. Since we work in good solvents, laterally homogeneous films are expected [62]. AFM pictures of dry films looked smooth. The rms roughness was about equal to the rms roughness of the substrate.

In general, it would certainly be desirable to infer structural information about the layers from the profiles in Fig. 4. Note that no *a priori* assumptions about the profile (e.g., parabolic [20,21]) can be made because the molecular weight distribution is not known with sufficient accuracy [63]. The determination of the density profile from the interaction with an AFM tip seems impossible for different reasons. First, the interactions probed represent a convolution of many interactions between different chains and different parts of the cantilever. Even if the geometric problem could be solved, a thorough understanding of the dynamical behavior as well as hydrodynamics involved would be needed. However, in application one is often primarily interested in the interaction rather than the structure of a polymer brush. A typical partner of interaction would, for instance, be a small colloidal particle. We consider the AFM tip as a model of a colloidal sphere interacting with the tethered layer. The dynamical interaction is of interest in itself, even though the structure of the brush can probably not be inferred from the interaction beyond some estimates of the brush thickness.

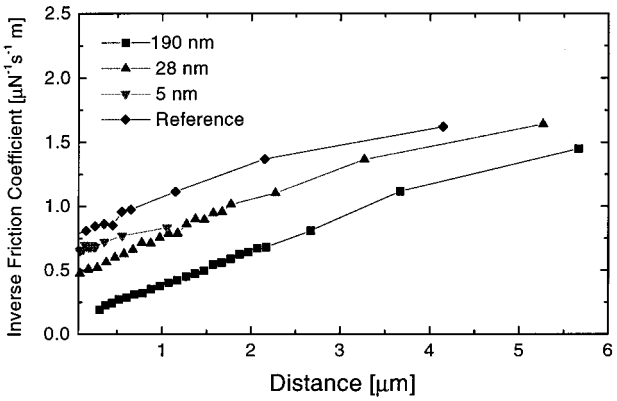

FIG. 5. The inverse of the friction coefficient $1/\xi$ vs distance D. At large distances simple lubrication would result in a straight line intersecting the abscissa at the ''hydrodynamic thickness'' [3,72]. As the figure shows, this simple picture does not apply.

Looking at the profiles in more detail, we find that the profile of the friction coefficient and the effective mass [Figs. 4(a) and 4(b)] are quite similar. They show a long-range interaction mediated by the liquid environment, which is present even for an empty glass slide. The long-range viscous interaction between AFM cantilevers and solid surfaces is discussed in detail in Refs. [44] and [64]. The viscous coupling to a surface results from the fact that the solvent can only escape sideways. In the presence of a polymer layer the increase in friction coefficient is much enhanced. A significant increase is observed even for $D = 2.5$ μm in the case of sample PMMA190. The profile of the dc force and the spring constant as well as mean-field calculations [21] make us believe that the brush itself does not significantly extend beyond $D = 1.5$ μm. However, the friction coefficient at $D = 2.5$ μm for sample PMMA190 is higher than the friction coefficient for an empty glass slide at $D = 1$ μm. 1 μm here corresponds to the difference between the position of the tip (2.5 μm) and what could be at most considered the ''outer edge'' of the brush. If one would place a ''virtual interface'' somewhere at the outer edge of the brush, this interface would still induce a higher friction in the movement of a nearby particle than an equivalent solid interface. In hydrodynamic terms, a virtual interface seems plausible. The location of that interface would be the ''hydrodynamic thickness,'' beyond which hydrodynamic screening is too strong to allow free draining of solvent. However, the virtual interface only gives the correct hydrodynamic boundary conditions, if it yields to vertical pressure, thereby dissipating en-

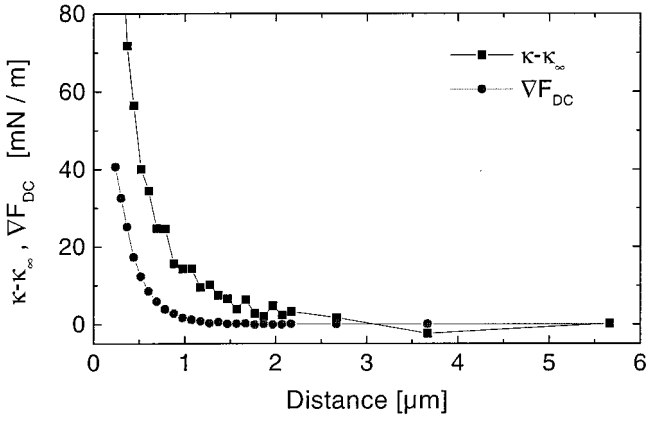

FIG. 6. Static force gradient $\nabla F_{\rm dc}$ and spring constant κ for sample PMMA190. The equality $\kappa-\kappa_\infty=\nabla F_{\rm dc}$ is not observed. In particular, the spring constant displays a tail at large distances not present in the profile of the dc force.

ergy. This motion of a tethered layer has been called the ''breathing mode'' [65–67].

In contrast to a solid surface, a brush may dissipate energy by letting itself be compressed vertically. A solid surface deviates all vertical flow to lateral motion without yielding vertically. This assumption is implicitly contained in the semiquantitative model by Güthner, Fischer, and Dransfeld [64] which was developed to model the near-field acoustic microscope. Vertical compression opens a channel of dissipation which is not present for solid interfaces.

Reynolds treated the friction coefficient of a sphere approaching a flat surface as early as 1886 [68]. In the derivation he assumed the ''lubrication limit,'' which states that the gap is much smaller than the other dimensions. He found that

$$\xi=\frac{6\pi\eta R^2}{D}=\xi_0\,\frac{R}{D}, \tag{4}$$

with R the sphere radius, D the gap width, and $\xi_0=6\pi\eta R$ the friction coefficient without a surface present. Equation (4) has been extensively tested experimentally [69–71]. Klein and co-workers modified Eq. (4) to take polymer layers into account [3,72]. They wrote

$$\frac{1}{\xi}=\frac{1}{\xi_0}\,\frac{D-2L_H}{R}, \tag{5}$$

with L_H the ''hydrodynamic thickness'' [73,74] of the brush. The factor of 2 occurs because both surfaces were covered by brushes in the experiments by Klein and co-workers [3,72]. When plotting $1/\xi$ vs D, a linear relation was observed at large distances. The extrapolation of this line to infinite friction (lubrication) yielded the hydrodynamic thickness. For the sake of comparison we display the inverse of the friction coefficient vs distance in Fig. 5. Clearly, Eq. (5) is not observed and the hydrodynamic thickness cannot be defined. Most likely this failure is due to the small size of the tip. The lubrication approximation is not fulfilled. We plan to glue small spheres to the tip in order to vary the effective radius R. It should be interesting to see at what sphere size the cross over to ordinary lubrication occurs. In particular, it should be interesting to see whether this critical radius depends on the brush thickness. This can be expected because the ''breathing modes'' presumably have a lateral extension of about the brush thickness [67].

The increase of effective mass qualitatively follows the friction coefficient. The effective mass is higher than the cantilever's proper mass because a part of the adjacent environment takes part in the movement, and therefore contributes to the system's inertia. The increase of effective mass with increasing friction is a consequence of accelerated motion. When the viscosity increases, the comoving volume increases and thereby the effective mass. The thickness of the comoving volume is in the order of the penetration depth of shear sound at the resonance frequency.

The decays of the DC force and the spring constant [Figs. 4(c) and 4(d)] are much steeper than the decay of the friction coefficient. The elastic interactions appear to be intrinsically short ranged. We do not find any long-range elastic interaction between an empty glass surface and an AFM tip. Comparing the profiles of DC force and spring constant, we find that the excess effective spring constant ($\kappa-\kappa_\infty$) is not equal to the derivative of the DC force $\nabla F_{\rm dc}$. This equality is usually observed in vacuum and is used as a contrast mechanism in the ''noncontact'' mode of the AFM. Figure 6 shows the force gradient $\nabla F_{\rm dc}$ and the excess spring constant $\kappa-\kappa_\infty$ for sample PMMA190 explicitly. The difference between static force gradient and effective spring constant probably originates in a time dependence of the elastic interaction. The existence of slow dynamics is independently indicated by the viscoelastic dispersion [45].

Interestingly, the difference between the static force gradient $\nabla F_{\rm dc}$ and the spring constant κ is most prominent in the tail of the profile of sample PMMA190. We find a significantly increased spring constant up to tip-sample distances of 1.5 μm, while the dc force decays to the bulk value at around 1 μm. We are not sure whether this proves that the segment density profile extends to 1.5 μm.

From the elastic interaction the thickness of the swollen brush can be assessed. The scaling and mean-field theories [13,14,20,21] predict that the thickness of a swollen brush scales as $h\sim(v/a^2)^{1/3}N$, with v the excluded volume parameter, a the grafting distance and N the number of monomers per chain. Inserting the numbers from Table I the scaling law predicts $h_{190}/h_{28}\sim 12$. From Fig. 4 we read that this ratio is between 10 and 15, depending on whether the spring constant or the dc force are used for assessing the brush thickness. The swelling ratios $h/h_{\rm dry}$ are 3 and 6 for samples PMMA28 and PMMA190, respectively.

Murat and Grest have recently calculated the dc force onto an AFM tip [54]. The tip was modeled as sphere sitting on a cylinder. They find that the force per unit area onto a small AFM tip is much weaker than the force onto a flat surface because the tip penetrates into the brush and laterally displaces the chains rather then compressing them vertically. We can qualitatively confirm that picture for samples PMMA5 and PMMA28 because we see a discontinuous disappearance of noise at a certain position. This is interpreted as the tip touching the substrate and is used for height calibration. For sample PMMA190 we do not find such a discontinuity. Apparently the tip is not able to penetrate to the

bottom of the brush. Note that the tip used in the calculation was cylindrical while our tip has pyramidal shape. A rough calculation of the compression modulus for Alexander brushes [29] yields higher forces than the ones we find experimentally. This also corroborates the interpretation that the tip dives into the brush.

CONCLUSIONS AND OUTLOOK

We have obtained static and dynamic force-distance profiles of tethered polymer layers swollen in a good solvent. The method relies on the spectral analysis of the noise of an AFM tip immersed into the layer. By fitting the noise spectra to Lorentzians, we obtain distance profiles of the friction coefficient, the effective spring constant, the effective mass, and the dc force. The profile of the effective mass closely follows the profile of the friction coefficient. The friction coefficient profiles display a long-range viscous interaction, which exceeds the viscous interaction between the cantilever and glass surface. We ascribe this increased interaction to the breathing mode. For sufficiently dense brushes, we observe a dc force and an increase in the effective spring constant. Both the dc force and the effective spring constant fall off with distance much faster than the friction coefficient. The increase in spring constant is not equal to the force gradient, which is attributed to the different time scales involved.

In the future, we want to increase our instrumental capabilities by reducing the electronic noise, reducing instrumental drifts, and enlarging the bandwidth. If a substantial gain in sensitivity can be achieved, two modifications of the experiment seem feasible. First, harder cantilevers can be used, which should allow dynamic investigations on harder interfaces like the surface of a weakly crosslinked rubber in air. Second, it should be possible to use larger tips and tips which carry a sphere at their outer end. This could simply be a glass sphere with the purpose of creating a well defined geometry. It could, however, also be a sphere covered with another brush or any kind of functional interface. It should be interesting to compare the static interaction of two brushes as measured with the surface forces apparatus to the dynamic interaction accessible with noise analysis of an AFM tip.

ACKNOWLEDGMENT

We gratefully acknowledge helpful discussions with Hans-Jürgen Butt.

[1] D. H. Napper, *Steric Stabilization of Colloidal Dispersions* (Academic, London, 1983).
[2] E. Raphaël and P. G. de Gennes, J. Phys. Chem. **96**, 4002 (1992).
[3] J. Klein, Annu. Rev. Mater. Sci. **26**, 581 (1996).
[4] J. Klein and E. Kumacheva, Science **269**, 816 (1995).
[5] J. H. van Zanten, Macromolecules **27**, 6797 (1994).
[6] R. S. Parnas and Y. Cohen, Rheol. Acta **33**, 485 (1994).
[7] M. Radmacher, R. W. Tillman, M. Fritz, and H. E. Gaub, Science **257**, 1900 (1992).
[8] G. J. Fleer, M. A. Cohen Stuart, J. M. H. M. Scheutjens, T. Cosgrove, and B. Vincent, *Polymers at Interfaces* (Chapman and Hall, London, 1993).
[9] A. Halperin, M. Tirell, and T. P. Lodge, Adv. Polym. Sci. **100**, 31 (1991).
[10] A. Halperin, in *Soft Order in Physical Systems*, Vol. 323 of *NATO Advanced Study Institute*, Series B: Physics, edited by Y. Rabin and R. Bruinsma (Plenum, New York, 1994), pp. 33–56.
[11] I. Szleifer and M. A. Cariggnano, Adv. Chem. Phys. **XCIV**, 165 (1996).
[12] G. S. Grest and M. Murat, in *Monte Carlo and Molecular Dynamics Simulations in Polymer Science*, edited by K. Binder (Clarendon, Oxford, 1994).
[13] S. Alexander, J. Phys. (Paris) **38**, 983 (1977).
[14] P. G. de Gennes, J. Phys. (Paris) **37**, 1443 (1976).
[15] P. Auroy, L. Auvray, and L. Leger, Phys. Rev. Lett. **66**, 719 (1991).
[16] P. Auroy, Y. Mir, and L. Auvray, Phys. Rev. Lett. **69**, 93 (1992).
[17] A. Karim, S. K. Satija, J. F. Douglas, J. F. Ankner, and L. J. Fetters, Phys. Rev. Lett. **73**, 3407 (1994).
[18] D. Perahia, D. G. Wiesler, S. K. Satija, L. J. Fetters, S. K. Sinha, and S. T. Milner, Phys. Rev. Lett. **72**, 100 (1994).
[19] A. Halperin, J. Phys. (Paris) **49**, 547 (1988).
[20] S. T. Milner, T. A. Witten, and M. Cates, Macromolecules **21**, 2610 (1988).
[21] E. B. Zhulina, O. V. Borisov, A. A. Pryamitsyn, and T. M. Birshtein, Macromolecules **24**, 140 (1991).
[22] G. S. Grest and M. Murat, Macromolecules **26**, 3108 (1993).
[23] P.-Y. Lai and K. Binder, J. Chem. Phys. **97**, 586 (1992).
[24] F. M. Haas, R. Hilfer, and K. Binder, J. Chem. Phys. **102**, 2960 (1995).
[25] A. Milchev and K. Binder, Macromolecules **29**, 343 (1996).
[26] H. J. Taunton, C. Toprackciogly, L. J. Fetters, and J. Klein, Macromolecules **23**, 571 (1990).
[27] J. B. Field, C. Toprakciogly, L. Dai, G. Hadziioannou, G. Smith, and W. Hamiltan, J. Phys. **2**, 2221 (1992).
[28] G. Hadziiannou, S. Patel, S. Granick, and M. Tirrell, J. Am. Chem. Soc. **108**, 2869 (1986).
[29] Y. Rabin and S. Alexander, Europhys. Lett. **13**, 49 (1990).
[30] J. L. Harden and M. E. Cates, Phys. Rev. E **53**, 3782 (1996).
[31] P. S. Doyle, E. S. G. Shaqfeh, and A. P. Gast, Phys. Rev. Lett. **78**, 1182 (1997).
[32] G. Binnig, C. F. Quate, and C. Gerber, Phys. Rev. Lett. **56**, 930 (1986).
[33] E. L. Florian, M. Radmacher, B. Fleck, and H. E. Gaub, Rev. Sci. Instrum. **65**, 639 (1994).
[34] P. Mailvald, H.-J. Butt, S. A. C. Gould, C. B. Prater, B. Drake, J. A. Gurley, V. B. Elins, and P. K. Hansma, Nanotechnology **2**, 103 (1991).
[35] J. Hu, X.-D. Xiao, D. F. Ogletree, and M. Salmeron, Surf. Sci. **344**, 221 (1995).
[36] E.-L. Florin, M. Radmacher, B. Fleck, and H. E. Gaub, Rev. Sci. Instrum. **65**, 639 (1994).

[37] Y. Martin, C. C. Williams, and H. K. Wickramasinghe, J. Appl. Phys. **61**, 4723 (1987).
[38] J. L. Hutter and J. Bechhoefer, Rev. Sci. Instrum. **64**, 1868 (1993).
[39] J. P. Cleveland, S. Manne, D. Bock, and P. K. Hansma, Rev. Sci. Instrum. **64**, 403 (1993).
[40] H.-J. Butt and M. Jaschke, Nanotechnology **6**, 1 (1995).
[41] H.-J. Butt, P. Siedle, K. Seifert, K. Fendler, T. Seeger, E. Bamberg, A. L. Weisenhorn, K. Goldie, and A. Engle, J. Microsc. **169**, 75 (1993).
[42] H.-J. Butt, M. Jaschke, and W. Ducker, Bioelectrochem. Bioenergetics **38**, 191 (1995).
[43] J. P. Cleveland, T. E. Schäffer, and P. K. Hansma, Phys. Rev. B **52**, R8692 (1995).
[44] A. Roters and D. Johannsmann, J. Phys.: Condens. Matter **8**, 7561 (1996).
[45] M. Gelbert, A. Roters, M. Schimmel, J. Rühe, and D. Johannsmann (unpublished).
[46] B. J. Alder and T. E. Wainwright, Phys. Rev. Lett. **18**, 988 (1967).
[47] J. Rühe, Habilitation-thesis, Universität Bayreuth, 1995.
[48] J. Rühe, Nachr. Chem. Tech. Lab. **42**, 1237 (1994).
[49] G. Tovar, S. Paul, W. Knoll, O. Prucker, and J. Rühe, Supramolecular Sci. **2**, 89 (1995).
[50] O. Prucker, Ph.D. thesis, Universität Bayreuth, 1995.
[51] M. Murat and G. S. Grest, Phys. Rev. Lett. **63**, 1074 (1989).
[52] R. Toral, A. Chakrabarti, and R. Dickman, Phys. Rev. E **50**, 343 (1994).
[53] R. M. Overney, D. P. Leta, C. F. Pictroski, M. H. Rafailovich, Y. Liu, J. Quinn, J. Sokolov, A. Eisenberg, and G. Overney, Phys. Rev. Lett. **76**, 1272 (1996).
[54] M. Murat and G. S. Grest, Macromolecules **29**, 8282 (1996).
[55] R. Kubo, M. Toda, and H. Hashitsume, *Statistical Physics* (Springer, Heidelberg, 1985), Vol. 2.
[56] B. Rothenhäusler, C. Duschl, and W. Knoll, Thin Solid Films **159**, 323 (1988).
[57] W. Hickel and W. Knoll, Appl. Phys. Lett. **57**, 1286 (1990).
[58] W. H. Press, S. A. Teukolsky, W. T. Vetterling, and B. P. Flannery, *Numerical Recipes in Pascal* (Cambridge University Press, Cambridge, 1990).
[59] D. Sarid, *Scanning Force Microscopy* (Oxford University Press, London, 1991), Chap. 3.
[60] J. E. Sader and L. White, J. Appl. Phys. **74**, 1 (1993).
[61] *CRC Handbook of Chemistry and Physics*, 66th ed., edited by R. C. Weast, M. J. Astle, and W. H. Beyer (CRC, Boca Raton FL, 1985).
[62] C. Yeung, A. C. Balazs, and D. Jasnow, Macromolecules **26**, 1914 (1993).
[63] S. T. Milner, T. A. Witten, and M. E. Cates, Macromolecules **22**, 853 (1989).
[64] P. Güthner, U. Ch. Fischer, and K. Dransfeld, Appl. Phys. B **48**, 89 (1989).
[65] G. Fytas, S. H. Anastasiadis, R. Seghrouchni, D. Vlassopoulos, J. Li, B. J. Factor, W. Theobald, and C. Toprakcioglu, Science **274**, 2041 (1996).
[66] P. G. de Gennes, Adv. Colloid Interface Sci. **27**, 189 (1987).
[67] G. H. Fredrickson, A. Ajdarai, L. Leibler, and J. P. Carton, Macromolecules **25**, 2882 (1992).
[68] O. Reynolds, Philos. Trans. R. Soc. London **177**, 157 (1886).
[69] J. Happel and H. Brenner, *Low Reynolds Number Hydrodynamics* (Prentice-Hall, Englewood Cliffs, NJ 1965).
[70] D. Y. C. Chan and R. G. Horn, J. Chem. Phys. **83**, 5311 (1985).
[71] J. N. Israelachvili, Colloid Polym. Sci. **264**, 1060 (1986).
[72] J. Klein, Y. Kamiyama, H. Yoshizawa, J. N. Israelachvili, P. Pincus *et al.*, Macromolecules **26**, 5552 (1993).
[73] J. L. Anderson, P. F. McKenzie, and R. M. Webber, Langmuir **7**, 162 (1991).
[74] R. M. Webber, C. C. van der Linden, and J. L. Anderson, Langmuir **12**, 1040 (1996).